PERGAMON

International Journal of Heat and Mass Transfer 45 (2002) 173–180

International Journal of HEAT and MASS TRANSFER

www.elsevier.com/locate/ijhmt

Comparison between local and homogenized models of radiative transfer in a set of parallel ducts considered as a porous medium

M. Tancrez [a], M. Hilka [b], J. Taine [a,*]

[a] *Laboratoire EM2C, École Centrale Paris – CNRS (UPR 288), Ecole Centrale Paris, 92295 Châtenay-Malabry Cedex, France*
[b] *Gaz de France, R&D Division, 93211 Saint Denis La Plaine BP 33 Cedex, France*

Received 28 March 2000; received in revised form 24 November 2000

Abstract

A set of parallel ducts of various cross-sections in a diffuse opaque solid medium is modeled as a continuous absorbing and isotropically scattering porous medium. Simple expressions of the absorption and scattering coefficients of this equivalent medium have been determined by identification of the Fourier transforms of the radiative power per unit volume, obtained from the continuous medium model and from a reference local model, in the case of an infinite system. Comparisons of radiative transfer results of the continuous medium model with those of the local model have been carried out for finite configurations typical of combustion applications. Typical discrepancies of a few percent have been observed both for the radiative power per unit volume and boundary radiative flux calculations. The continuous medium model, although practically equivalent to the local model, leads to much faster computation.

1. Introduction

Many recent studies, e.g. [1–9], deal with combustion within porous media and a survey has been given by Howell et al. [1]. It has been emphasized that the radiative transfer inside the porous medium plays an important role in the flame stabilization [2,5] and that scattering effects cannot be neglected [3]. In particular, radiative loss plays a prominent role in the case of radiative porous heaters.

The modeling of the radiative transfer at a microscopic scale in a porous structure, taking into account absorption and reflection phenomena, can be difficult. Consequently, a porous medium is often treated as a continuous homogeneous absorbing and scattering medium. Different types of radiative methods have been used. A simple model consists of linearizing the radiative transfer inside the porous medium by considering an equivalent conductivity that takes into account both absorption and scattering at the optically thick medium limit [8,10]. If the porous medium is considered as nonscattering, the radiative transfer equation can be solved by using E_n functions [5,11]. Radiative transfer can also be treated by a P_n method, e.g. [2,3,6], a discrete ordinates method, e.g. [12], or a S_n method [13]. The classical Schuster–Schwarzschild method [14–16] allows scattering to be simply accounted for [4,17]. Many radiative models have been detailed by Kaviany [18]. In all these methods, the absorption and scattering coefficients and the phase function are assumed to be known. In practice, they are estimated from either simple geometrical considerations, experimental studies, e.g. [1,19] or from a Monte Carlo approach, e.g. [20].

The present paper deals only with radiative transfer in a set of parallel diffuse opaque ducts used, for instance, in catalytic burners. As the system structure is simple, radiative transfer can be modeled at the local duct scale from the incident and leaving intensity method [16,21]. But the implementation of this approach, referred to here as the local model, requires an

* Corresponding author. Tel.: +33-1-41-13-10-63; fax: +33-1-47-02-80-35.
E-mail address: taine@em2c.ecp.fr (J. Taine).

0017-9310/02/$ - see front matter
PII: S0017-9310(01)00116-8

Nomenclature

$\mathscr{A} = 2/R_h$	interfacial area per unit volume of the fluid phase
E	least-square error
$\mathscr{E}$	relative discrepancy
$f\,dx, F, g$	view factors
I_ν	spectral radiative intensity
k	length to width ratio for a rectangular cross-section
l	characteristic length of a cross-section
p_ν	spectral phase function
P_ν	spectral radiative power per unit volume of the fluid phase
$\mathscr{P}$	cross-section perimeter
$\mathscr{S}$	cross-section area
$R_h = 2\mathscr{S}/\mathscr{P}$	hydraulic radius
T	temperature
x, x'	position in the direct space
$X = x' - x$	distance in the direct space
$X^+ = X/l$	nondimensional distance

Greek symbols

$\beta_\nu = \kappa_\nu + \sigma_\nu$	spectral extinction coefficient
ϵ_ν	spectral emissivity
$\gamma = \sqrt{2R_h\beta}$	nondimensional parameter
κ_ν	spectral absorption coefficient
ω	conjugated variable in the Fourier space
Π	porosity of the medium
σ_ν	spectral scattering coefficient
σ_B	Stefan constant

Subscripts

m	optimal coefficient (least-square minimization)
ν	spectral
w, 1, 2	wall, left wall, right wall

Superscripts

e	emitted
i	incident
l	leaving
+	characterizing the propagation in the x^+ direction
−	characterizing the propagation in the x^- direction
~	Fourier transformed function

significant CPU time, which is a major drawback when many iterations have to be carried out due to the coupling of radiation with conduction, convection and combustion in the considered application. Consequently, a much faster approach, based on an equivalent homogenized continuous medium, characterized by a porosity and considered to emit, absorb and scatter radiation, has been developed here.

The first aim of this work, developed in Section 2, is to characterize the absorption and scattering coefficients of the equivalent continuous medium from the actual properties of the ducts. Four configurations of temperature fields and thermal boundary conditions, typical of actual systems, are then considered in order to validate the continuous approach by comparison with the local model. The radiative power per unit volume of the fluid phase and the radiative fluxes at the boundaries, calculated by the two approaches, are compared in Section 3. Finally, conclusions are drawn.

2. Identification method

The system considered in this section is an infinite opaque solid medium of spectral diffuse emissivity ϵ_ν, with a set of parallel ducts of constant cross-section (circular, rectangular or regular polygonal) passing through, as shown in Fig. 1. The characteristic width of a cross-section is l. The gas which flows through the ducts is assumed tranparent. Indeed, for the catalytic burners considered here, the product of the absorbing-emitting gas partial pressure by a typical length of the system is less than 10^{-3} m atm; in these conditions absorption is negligible [22].

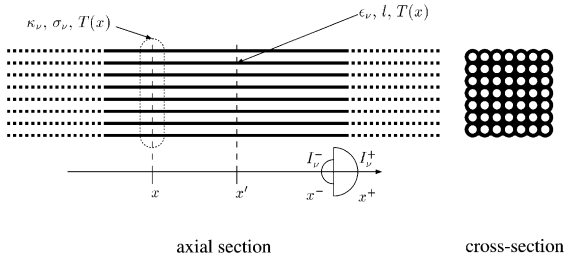

Fig. 1. Definition of the considered system.

Radiative transfer in such a system can be calculated by two approaches : (i) directly, from the determination of the incident and leaving spectral intensities at the duct walls (local approach); (ii) by a simple transfer model applied to an equivalent continuous medium characterized by the absorption and scattering coefficients κ_ν and σ_ν and an isotropic phase function. This model will be discussed later. κ_ν and σ_ν have to be expressed in terms of ϵ_ν and l by identification of the expressions of the

radiative power per unit volume of the fluid phase obtained by the two previous approaches. The choice of an infinite system eliminates the boundary condition problem, studied in Section 3.

The spectral radiative power per unit volume of the fluid phase, $P_v(x)$, is written, in the local approach

$$P_v(x) = \mathscr{A}\pi\left[I_v^{\mathrm{i}}(x) - I_v^{\mathrm{l}}(x)\right], \tag{1}$$

where $\mathscr{A}$ is the interfacial area per unit volume of fluid and $I_v^{\mathrm{l}}(x)$ and $I_v^{\mathrm{i}}(x)$ are respectively the leaving and incident isotropic intensities, at a point x of a duct, given by [16,21]

$$I_v^{\mathrm{l}}(x) = \epsilon_v I_v^{\mathrm{o}}(x) + (1-\epsilon_v) I_v^{\mathrm{i}}(x), \tag{2}$$

$$I_v^{\mathrm{i}}(x) = \int_{-\infty}^{+\infty} f(x-x') I_v^{\mathrm{l}}(x')\,\mathrm{d}x' = \left(f \otimes I_v^{\mathrm{l}}\right)(x), \tag{3}$$

where $I_v^{\mathrm{o}}(x)$ is the equilibrium intensity at the point x, of temperature $T(x)$, and $f(x-x')\,\mathrm{d}x$ the differential view factor between two differential ring elements $(x, x+\mathrm{d}x)$ and $(x', x'+\mathrm{d}x')$. Taking the Fourier transform which is defined for any function $h(x)$

$$\tilde{h}(\omega) = \int_{-\infty}^{+\infty} h(x)\exp(-2\pi j\omega x)\,\mathrm{d}x, \tag{4}$$

leads to the expression

$$\widetilde{P}_v = -\frac{\mathscr{A}\epsilon_v\left[1-\widetilde{f}(\omega)\right]}{1-(1-\epsilon_v)\widetilde{f}(\omega)}\pi\widetilde{I_v^{\mathrm{o}}(T)}(\omega), \tag{5}$$

which is the direct solution of the problem in Fourier space.

On the other hand, an expression similar to Eq. (5) can be obtained from the continuous medium approach and the Schuster–Schwarzschild [14–16,18] simple model. This model assumes that intensity is isotropic in the two half spaces corresponding to x^+ and x^- propagating directions, as shown in Fig. 1. The corresponding values are called I_v^+ and I_v^-, respectively.

In the continuous medium approach, the choice of an isotropic phase function is justified by the following: (i) as the actual geometry and duct reflectivity are symmetrical with respect to a plane perpendicular to the ducts, the phase function is symmetrical; (ii) an isotropic phase function is consistent with the choice of the Schuster–Schwarzschild method in which only hemispherical fluxes are considered; (iii) the hypothesis of isotropic scattering is consistent with diffuse duct reflectivity.

All the previous assumptions lead to a system of two coupled averaged radiative transfer equations [16,21],

$$\frac{\mathrm{d}I_v^+}{\mathrm{d}x} = -2\beta_v I_v^+ + 2\kappa_v I_v^{\mathrm{o}}(x) + (\beta_v - \kappa_v)(I_v^+ + I_v^-), \tag{6}$$

$$-\frac{\mathrm{d}I_v^-}{\mathrm{d}x} = -2\beta_v I_v^- + 2\kappa_v I_v^{\mathrm{o}}(x) + (\beta_v - \kappa_v)(I_v^+ + I_v^-), \tag{7}$$

where β_v is the extinction coefficient ($\beta_v = \kappa_v + \sigma_v$). The radiative power per unit volume of the fluid phase averaged over a representative volume element is then

$$P_v = -\pi\frac{\mathrm{d}}{\mathrm{d}x}(I_v^+ - I_v^-) \tag{8}$$

and, after taking the Fourier transform, we obtain

$$\widetilde{P}_v = -\frac{4\kappa_v\pi^2\omega^2}{\beta_v\kappa_v + \pi^2\omega^2}\pi\widetilde{I_v^{\mathrm{o}}(T)}(\omega). \tag{9}$$

The solution for κ_v is simple if we consider the two following expressions of the emitted spectral power per unit volume of the fluid phase:

$$P_v^{\mathrm{e}} = \mathscr{A}\pi\epsilon_v I_v^{\mathrm{o}}(T) = 4\pi\kappa_v I_v^{\mathrm{o}}(T), \tag{10}$$

which lead to

$$\kappa_v = \mathscr{A}\epsilon_v/4. \tag{11}$$

It is worth noting that this result can also be obtained by identification of Eqs. 5 and 9 at the infinite ω limit, which corresponds in the direct space to local properties and for which $\widetilde{f}(\omega) \to 0$.

In order to obtain β_v, the expressions of the radiative power per unit volume of the fluid phase, given by Eqs. (5) and (9), are identified, which leads to

$$\widetilde{f} = 1/\left(1 + \epsilon_v\pi^2\omega^2/\beta_v\kappa_v\right) \tag{12}$$

and, after taking the inverse Fourier transform, to

$$f(X) = \sqrt{\beta_v\kappa_v/\epsilon_v}\exp\left(-2\sqrt{\beta_v\kappa_v/\epsilon_v}X\right), \tag{13}$$

where X designates $|x'-x|$. $f(X)$ can also be directly obtained from $g(X)$, the view factor between two cross-section areas of a cylindrical duct,

$$f(X) = \frac{\mathscr{S}}{\mathscr{P}}\frac{\mathrm{d}^2 g}{\mathrm{d}X^2}(X), \tag{14}$$

where $\mathscr{S}$ and $\mathscr{P}$ are respectively the area and the perimeter of the cross-sections. $f(X)$ can be expressed analytically or numerically for circular, rectangular [16,21], and polygonal [23] cross-sections. We obtain an expression of β_v, for each geometry, after identification of Eqs. (13) and (14).

These expressions are now written in a nondimensional form by introducing the hydraulic radius $R_{\mathrm{h}} = 2\mathscr{S}/\mathscr{P}$ and the nondimensional length $X^+ = X/R_{\mathrm{h}} = |x'-x|/R_{\mathrm{h}}$, i.e.

$$2R_{\mathrm{h}}f(X^+) = \frac{\mathrm{d}^2 g}{\mathrm{d}X^{+2}}(X^+) = \gamma\exp[-\gamma X^+] \tag{15}$$

in which γ is a nondimensional parameter that is independent of radiation frequency

$$\gamma = 2R_{\mathrm{h}}\sqrt{\beta_v\kappa_v/\epsilon_v} = R_{\mathrm{h}}\sqrt{\mathscr{A}\beta}. \tag{16}$$

Table 1
γ_m values for a rectangular section

k	γ_m	$100E(\gamma_m)$
1	1.05	7
2	1.07	6
5	1.12	5
10	1.14	6
100	1.17	8
∞	1.18	8

Table 2
γ_m values for different cross-sections

	γ_m	$100E(\gamma_m)$
Triangle	1.06	2
Square	1.06	1.4
Pentagon	1.05	1.5
Hexagon	1.05	1.5
Octagon	1.07	3.9
Circle	1.05	3

Consequently, β is also independent of radiation frequency.

For a given geometry, Eqs. (5) and (9) lead to identical results if there is a γ_m value such as $\gamma_m \exp[-\gamma_m X^+]$ is approximately equal to $2R_h f(X^+)$ in the variation range of X^+, as developed in Appendix A. The optimal γ_m value is obtained by a least-square-fit method, i.e., by minimizing the quantity

$$E(\gamma) = \left\{ \frac{\int_0^\infty [2R_h f(X^+) - \gamma \exp(-\gamma X^+)]^2 \, dX^+}{\int_0^\infty [2R_h f(X^+)]^2 \, dX^+} \right\}^{1/2}. \quad (17)$$

In these conditions, the expressions of κ_v, β_v and σ_v in terms of ϵ_v and R_h become

$$\kappa_v = \epsilon_v/(2R_h), \quad \beta = \gamma_m^2/(2R_h), \quad \sigma_v = (\gamma_m^2 - \epsilon_v)/(2R_h). \quad (18)$$

The view factor expressions for the considered configurations are given in Appendix A. Optimized values γ_m are given in Table 1 for rectangular cross-sections and in Table 2 for regular polygonal and circular cross-sections. Discussions related to the method of determination of γ_m are reported in Appendix A.

In conclusion, as shown in Tables 1 and 2, for aspect ratio values that are not too large, a recommended value of γ_m is 1.05. The extinction length β^{-1}, given by Eq. (18), is then equal to Hottel's equivalent radius for an infinite cylinder $1.8R_h$ [16,21]. This surprising result can be easily understood in the case $\rho_v = 1 - \epsilon_v = 1$ (extinction is only due to diffuse reflection).

3. Comparison of the two model results

The local and the continuous medium models are implemented in this section for the following system : (i) the set of cylindrical ducts, of porosity Π lies between $x = 0$ and $x = L = 1$ cm. A transparent fluid flows in this set of identical parallel ducts of circular cross-sections of radius R_h; (ii) the solid phase is gray, of emissivity ϵ; κ and σ are obtained from Eq. (18) and Table 2; (iii) the solid phase is characterized by a temperature profile $T(x)$; (iv) the cylindrical ducts lay between two gray opaque walls of respective temperatures T_1 and T_2, and diffuse emissivities ϵ_1 and ϵ_2, respectively, as shown in Fig. 2.

In the local model, we consider the isotropic intensities leaving and entering a duct at $x = L$, called I_L^l and I_L^i, respectively, i.e.

$$I_L^i = \epsilon_2 I^o(T_2) + (1 - \epsilon_2) I_2^i, \quad (19)$$

$$I_L^l = \int_0^L F(x \to L) I^l(x) 2 \, dx/R_h + F(0 \to L) I_0^i, \quad (20)$$

where I_0^i is the entering intensity at $x = 0$ and I_2^i the incident intensity at wall 2

$$I_2^i = \Pi I_L^l + (1 - \Pi)\{\epsilon I^o[T(L)] + (1 - \epsilon) I_L^i\} \quad (21)$$

and where $F(x \to L)$ and $F(0 \to L)$ are the view factors between a differential ring element dx and the cross-section area $x = L$, and between the two cross-section areas $x = 0$ and $x = L$, respectively. It is worth noting that $I^l(x)$ in Eq. (20) depends also on I_0^i and I_L^i, by Eq. (2) and on the modified expression of Eq. (3), i.e.

$$I^i(x) = \int_0^L f(|x - x'|) I^l(x') \, dx' + F(x \to 0) I_0^i + F(x \to L) I_L^i. \quad (22)$$

In Eqs. (19)–(22), we have assumed that the incident and leaving intensities are uniform and isotropic at $x = 0$, $x = L$ and at boundary walls. Similar boundary conditions are considered at $x = 0$. Finally, for a given temperature field, the whole set of boundary conditions leads to a complex system of linear equations for I_L^i, I_L^l, I_0^i, I_0^l.

For the equivalent absorbing and scattering medium, the boundary condition at the cross-section $x = L$ is

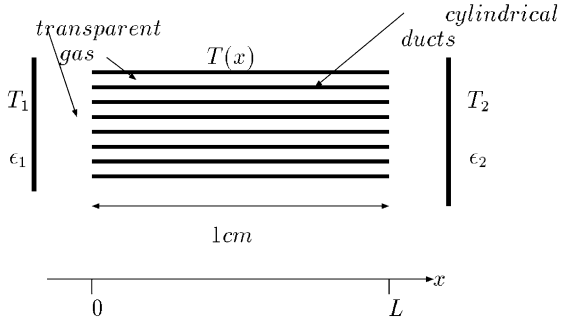

Fig. 2. The finite configuration.

given by Eqs. (19) and (21) if $I^+(L)$ and $I^-(L)$ are substituted to I_L^{l} and I_L^{i}, respectively.

In order to validate the continuous medium model in comparison to the local model, four configurations are considered in the following, characterized by different temperature fields in the ducts, and different opaque wall temperatures, as shown in Fig. 3. The two last configurations are typical of combustion. Other parameters are defined by $\Pi = 0.85$, $\epsilon = 0.5$, $R_{\mathrm{h}} = 5 \times 10^{-2}$ cm, $\epsilon_1 = 0.9$, $\epsilon_2 = 0.9$ and $L = 1$ cm, which leads to $\kappa = 5\ \mathrm{cm}^{-1}$, $\sigma = 6\ \mathrm{cm}^{-1}$ and $\beta = 11\ \mathrm{cm}^{-1}$. The first case deals with an isothermal system between two cold walls; case 2 with a system characterized by a large temperature gradient at $x = 0.5$ cm; the boundary conditions are chosen in such a manner that the radiative fluxes at the walls are weak. In case 3, the temperature field is the same as in case 2, but the boundary conditions are chosen in such a manner that the radiative fluxes at the right opaque wall are significant. Case 4 deals with a temperature gradient close to a wall. The highest temperature for each configuration is $T_{\max} = 1500$ K.

For each configuration, the radiative power per unit volume of fluid obtained with the continuous medium approach, called $P_{\mathrm{cm}}(x)$, is compared: (i) with the corresponding result obtained with the standard local model, considered as reference and called $P_{\mathrm{ref}}(x)$; (ii) with the result obtained with a local model using the approximate differential view factor given by Eq. (15), called $P_\gamma(x)$. This last approach is considered in order to emphasize the contribution of the approximate expression of the view factor (Eq. (15)) to the global error introduced by the continuous medium model. The total nondimensional radiative power per unit volume of fluid $P^*_{\mathrm{ref}} = P_{\mathrm{ref}}/(\mathscr{A}\epsilon\sigma_B T^4_{\max})$ obtained with the reference local approach is plotted in Figs. 4–7. The relative discrepancies obtained with the approximate local model and

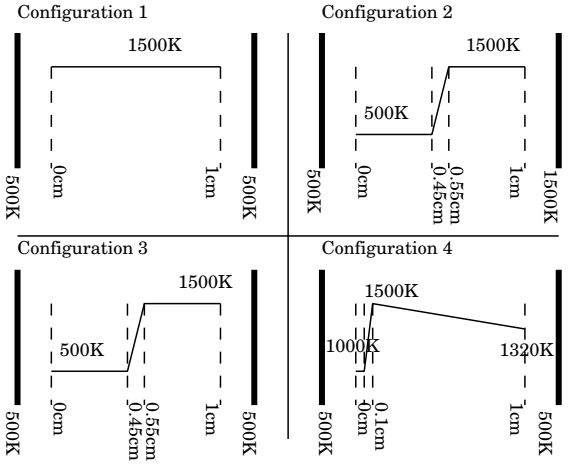

Fig. 3. The four configurations studied.

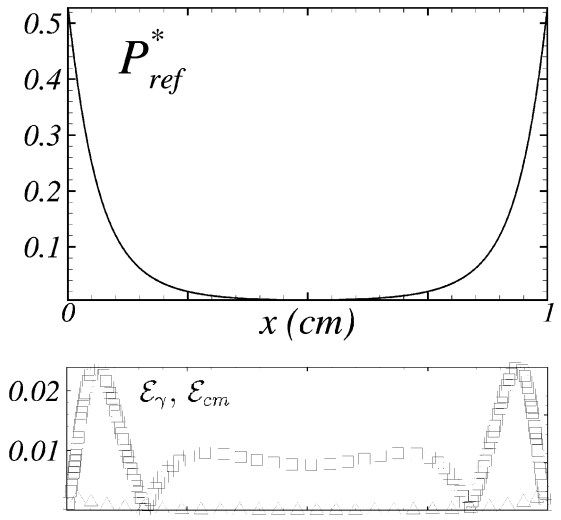

Fig. 4. Configuration 1. Nondimensional radiative power per unit volume of fluid P^*_{ref} obtained with the standard local model (–) and relative discrepancies $\mathscr{E}_\gamma$ (□) and $\mathscr{E}_{\mathrm{cm}}$ (△) vs x in the medium.

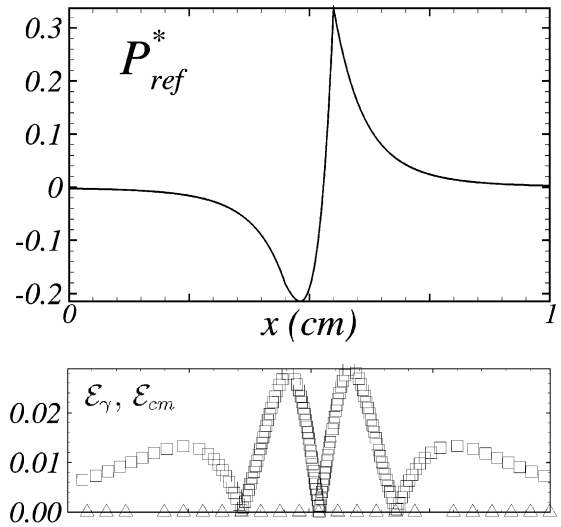

Fig. 5. Configuration 2. Nondimensional radiative power per unit volume of fluid P^*_{ref} obtained with the standard local model (–) and relative discrepancies $\mathscr{E}_\gamma$ (□) and $\mathscr{E}_{\mathrm{cm}}$ (△) vs x in the medium.

the continuous medium model, $\mathscr{E}_\gamma = |P_\gamma(x) - P_{\mathrm{ref}}(x)|/P^{\max}_{\mathrm{ref}}$ and $\mathscr{E}_{\mathrm{cm}} = |P_{\mathrm{cm}}(x) - P_\gamma(x)|/P^{\max}_{\mathrm{ref}}$, where $P^{\mathrm{ref}}_{\max}$ is the maximal value of P_{ref}, are also plotted. For these calculations 5000 regularly spaced grid points, have been used.

Figs. 4–7 show that, in all considered cases, $\mathscr{E}_\gamma$ is always much larger than $\mathscr{E}_{\mathrm{cm}}$ but typically less than 0.03. The continuous medium model accuracy is only limited

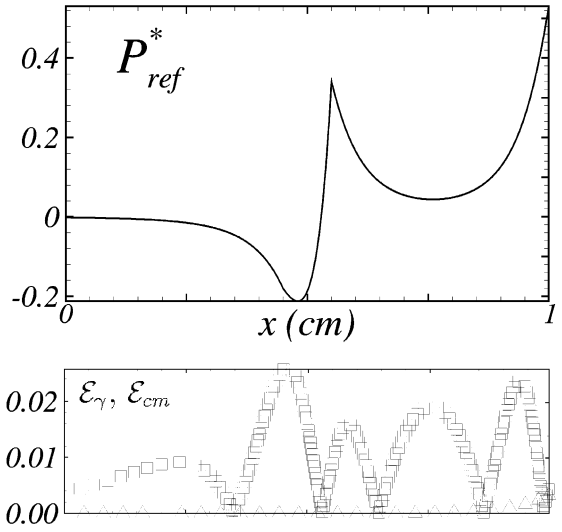

Fig. 6. Configuration 3. Nondimensional radiative power per unit volume of fluid P^*_{ref} obtained with the standard local model (–) and relative discrepancies $\mathscr{E}_\gamma$ (□) and $\mathscr{E}_{\mathrm{cm}}$ (△) vs x in the medium.

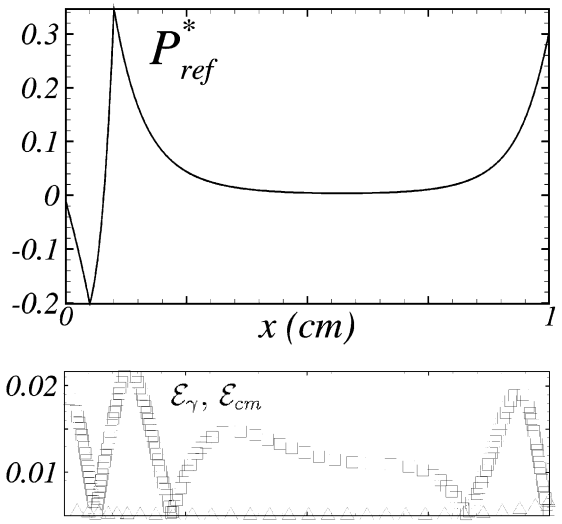

Fig. 7. Configuration 4. Nondimensional radiative power per unit volume of fluid P^*_{ref} obtained with the standard local model (–) and relative discrepancies $\mathscr{E}_\gamma$ (□) and $\mathscr{E}_{\mathrm{cm}}$ (△) vs x in the medium.

by the accuracy of the approximate view factor expression (Eq. (15)). Indeed, the actual view factor cannot be rigorously replaced by an exponential law. The main advantage of the continuous medium model is that it requires a computation time proportional to N, the number of grid points, without iteration. On the other hand, the local approach requires multiple iterations and a computation time proportional to N^2 per iteration.

The values of the nondimensional radiative flux $\varphi^R/(\sigma_B T^4_{\max})$ obtained with the three approaches are given in Table 3. No significant discrepancy appears between the continuous medium model and the local model based on Eq. (15). The continuous medium model leads to accurate flux results for configurations 1, 3 and 4, when wall fluxes are large. The relative discrepancy $|\varphi_{\mathrm{cm}} - \varphi_{\mathrm{ref}}|/\varphi_{\mathrm{ref}}$ is less than 0.03 for these cases. When the boundary flux is practically null (configuration 2 and left side of configuration 3), the relative discrepancy is large, but this case is without practical importance. This discrepancy results from discrepancy between Eq. (15) and the actual view factor expression for large x values.

4. Conclusion

This study has shown the practical equivalence between a Schuster–Schwarzschild model applied to an equivalent homogenized continuous medium and a reference local model to calculate radiative transfer in a set of ducts passing through an opaque solid medium at high temperature. Absorption and scattering coefficients of the equivalent isotropically scattering continuous medium have simple expressions. The approximated model leads to a typical relative accuracy of a few percent and only requires a CPU time proportional to N, the number of grid points, without iteration, instead of N^2 per iteration in the case of the reference model.

Table 3
Nondimensional radiative flux $\varphi^R/(\sigma_B T^4_{\max})$ at the two opaque walls

	Case 1		Case 2		Case 3		Case 4	
	Left	Right	Left	Right	Left	Right	Left	Right
Standard local model	0.712	0.712	8.56×10^{-3}	1.04×10^{-2}	6.67×10^{-3}	0.704	0.308	0.444
Approximate local model	0.708	0.708	4.3×10^{-4}	7.7×10^{-4}	4.3×10^{-4}	0.708	0.298	0.438
Continuous medium model	0.708	0.708	4.3×10^{-4}	7.7×10^{-4}	4.3×10^{-4}	0.708	0.299	0.439

Acknowledgements

M. Tancrez acknowledges the financial support of ADEME and Gaz de France for his work of "Thèse de Doctorat".

Appendix A

For ducts of circular cross-sections, the view factor $g(X^+)$ is [16,21]

$$g_{\mathrm{circ}}(X^+) = \left(2 + X^{+2} - \sqrt{4X^{+2} + X^{+4}}\right)\Big/2. \tag{A.1}$$

Direct results of the optimization defined by Eq. (17) and obtained by using Eq. (14) are reported in Table 2.

For ducts of rectangular cross-sections, the view factor between two rectangles of length L and width $W = kL$ is given by [16,21]

$$\begin{aligned} y &= W/X, \\ z &= L/X, \\ g_{\mathrm{rec}}(y,z) &= \left(\ln\left[(1+y^2)(1+z^2)/(1+y^2+z^2)\right]\right)/(\pi yz) \\ &\quad + 2\left[\sqrt{1+z^2}\tan^{-1}\left(y/\sqrt{1+z^2}\right)\right]\Big/(\pi z) \\ &\quad + 2\left[\sqrt{1+y^2}\tan^{-1}\left(z/\sqrt{1+y^2}\right)\right]\Big/(\pi y) \\ &\quad - 2\tan^{-1}(y)/(\pi z) - 2\tan^{-1}(z)/(\pi y). \end{aligned} \tag{A.2}$$

Direct results of the optimization defined by Eq. (17) and obtained by using Eq. (14), for different values of k are reported in Table 1. When $k \to \infty$, Eq. (A.2) becomes [16,21] $g_{\mathrm{pla}}(X^+) = \sqrt{1+X^{+2}} - X^+$. Results are reported in Table 1.

For ducts of regular polygonal cross-sections (triangle, square, pentagon, hexagon, octagon), the analytical expression of $g(X^+)$ is too complex to be used, but these view factors have been tabulated by Feingold [23] as shown in Fig. 8. It appears that the expressions of these view factors are close to Eq. (A.1) related to circles. Consequently approximate expressions $g^*(X^+)$ of $g_{\mathrm{pol}}(X^+)$, for ducts of regular polygonal cross-sections, have been established under a form close to Eq. (A.1), i.e.

$$g^*(X^+) = \left(a_1 + a_2 X^{+2} - \sqrt{a_3 X^{+2} + a_4 X^{+4}}\right)\Big/2 \tag{A.3}$$

by a discrete least-square fitting method. For the configurations considered $\left[\int_0^\infty (g-g^*)^2\,\mathrm{d}X^+ / \int_0^\infty g^2\,\mathrm{d}X^+\right]^{1/2}$ is lower than 0.04. This procedure applied to circular cross-section leads to Eq. (A.1) with a typical relative accuracy of 0.01 on parameters a_i.

In a second step, the values γ_m^* which minimize the criterion

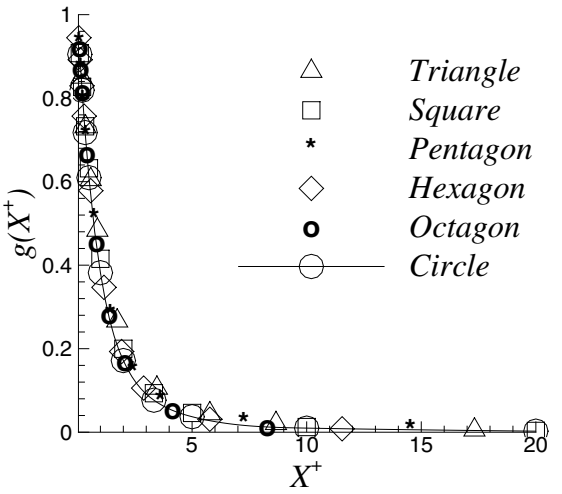

Fig. 8. View factors for regular polygons.

$$E^*(\gamma^*) = \left\{ \frac{\sum_i \left[\mathrm{d}^2 g^*/\mathrm{d}X^{+2}(X_i^+) - \gamma^* \exp\left(-\gamma^* X_i^+\right)\right]^2}{\sum_i \left[\mathrm{d}^2 G/\mathrm{d}X^{+2}(X_i^+)\right]^2} \right\}^{1/2} \tag{A.4}$$

have been calculated and reported in Table 2.

References

[1] J.R. Howell, M.J. Hall, J.L. Ellzey, Combustion of hydrocarbon fuels within porous inert media, Prog. Energ. Combust. Sci. 22 (1996) 121–145.
[2] S.B. Sathe, R.E. Peck, T.W. Tong, Flame stabilisation and multimode heat transfer in inert porous media: a numerical study, Combust. Sci. Technol. 70 (1989) 93–109.
[3] T.W. Tong, S.B. Sathe, Heat transfer characteristics of porous radiant burners, J. Heat Transfer 113 (1991) 423–428.
[4] F. Andersen, Heat transport model for fibre burners, Prog. Energ. Combust. Sci. 18 (1991) 1–12.
[5] Y. Yoshizawa, K. Sasaki, R. Echigo, Analytical study of the structure of radiation controlled flame, Int. J. Heat Mass Transfer 31 (2) (1988) 311–319.
[6] M. Maalouf, J.F. Leone, A. Lallemand, Transfert thermique en milieu réactionnel fibreux, Revue Générale de Thermique 363 (1988) 166–171.
[7] M.D. Rumminger, Numerical and experimental investigation of heat transfer and pollutant formation in porous direct-fired radiant burners, Ph.D. thesis, University of California, Berkeley, 1996.
[8] S.A. Zhdanok, K.V. Dobrego, S.I. Futko, Flame localization inside axis-symmetric cylindrical and spherical porous media burners, Int. J. Heat Mass Transfer 41 (1998) 3647–3655.
[9] V.V. Martinenko, R. Echigo, H. Yoshida, Mathematical model of self-sustaining combustion in inert porous

medium with phase change under complex heat transfer, Int. J. Heat Mass Transfer 41 (1) (1998) 117–126.
[10] X.-G. Liang, W. Qu, Effective thermal conductivity of gas–solid composite materials and temperature difference effect at high temperature, Int. J. Heat Mass Transfer 42 (1999) 1885–1893.
[11] R. Echigo, S. Hasegawa, S. Nakano, Simultaneous radiative and convective heat transfer in a packed bed with high porosity, JSME 40 (1974) 479, Translated by Ryozo Echigo.
[12] T.J. Hendricks, J.R. Howell, New radiative analysis approach for reticulated porous ceramics using discrete ordinates method, J. Heat Transfer 118 (1996) 911–917.
[13] J.M. Zhang, W.H. Sutton, F.C. Lai, Enhancement of heat transfer using porous convection-to-radiation converter for laminar flow in a circular duct, Int. J. Heat Mass Transfer 40 (1) (1997) 39–48.
[14] A. Schuster, Radiation through a foggy atmosphere, Astrophys. J. 21 (1905) 1–22.
[15] K. Schwarzschild, Equilibrium of the sun's atmosphere, Ges. Wiss. Gottingen. Nachr., Math-Phys. Klasse 1 (1906) 41–53.
[16] J. Taine, J.P. Petit, Transferts Thermiques, third ed., Dunod, Paris (in press).
[17] H. Yoshida, J.H. Yun, R. Echigo, Transient characteristics of combined conduction convection, and radiation heat transfer in porous media, Int. J. Heat Mass Transfer 33 (5) (1990) 847–857.
[18] M. Kaviany, Principles of Heat Transfer in Porous Media, second ed., Springer, Berlin, 1999.
[19] D. Baillis, M. Raynaud, J.F. Sacadura, Spectral radiative properties of open cell foam insulation, J. Thermophys. Heat Transfer 13 (1999) 292–298.
[20] C. Argento, D. Bouvard, A ray tracing method for evaluating the radiative heat transfer in porous media, Int. J. Heat Mass Transfer 39 (15) (1996) 3175–3180.
[21] R. Siegel, J.R. Howell, Thermal Radiation Heat Transfer, third ed., Taylor and Francis, London, 1992.
[22] J. Taine, A. Soufiani, Gas IR radiative properties: from spectroscopic data to approximate models, Adv. Heat Transfer 33 (1999) 295–414.
[23] A. Feingold, Radiant-interchange configuration factors between various selected plane surface, Proc. R. Soc. London Ser. A, 1966.